ACS APPLIED MATERIALS & INTERFACES

Research Article

www.acsami.org

Sandwich Approach toward Inverse Opals with Linear and Nonlinear Optical Functionalities

Pieter-Jan Demeyer,* Stefaan Vandendriessche, Stijn Van Cleuvenbergen, Sophie Carron, Kevin Bogaerts, Tatjana N. Parac-Vogt, Thierry Verbiest, and Koen Clays*

University of Leuven, Department of Chemistry, Celestijnenlaan 200D & 200F, 3001 Heverlee, Flemish Brabant, Belgium

Supporting Information

ABSTRACT: Three-dimensionally ordered macroporous materials have unique structural and optical properties, making them useful for numerous applications in catalysis, membrane science, and optics. Accessible and economic fabrication of these materials is essential to fully explore the many possibilities that these materials present. A new templating method to fabricate three-dimensionally ordered macroporous materials without overlayers is presented. The resulting structures are freestanding inverse opals with large-area uniformity. The versatility and power of our fabrication method is demonstrated by synthesizing inverse opals displaying fluorescence, chirality, upconversion, second harmonic generation, and third harmonic generation. This economical and versatile fabrication method will facilitate research on inverse opals in general and on linear and nonlinear optical effects in 3D photonic crystals specifically. The relative ease of synthesis and wide variety of resulting materials will help the characterization and improvement of existing anomalous dispersion effects in these structures, while providing a platform for the discovery and demonstration of novel effects.

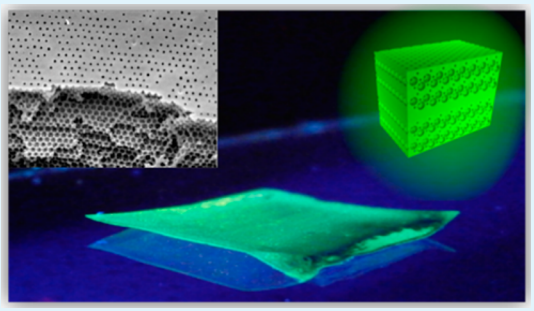

KEYWORDS: *macroporous materials, inverse opals, nonlinear optics, photonic crystals, templating, polymer doping*

1. INTRODUCTION

Three-dimensionally (3D) ordered macroporous materials combine interesting structural and optical properties.[1−3] Their porous nature provides a high surface area, which is interesting for catalysis,[4,5] and can also be exploited in storage units and membrane sciences.[6] Moreover, the 3D order gives rise to unique optical properties such as photonic band gap effects, which selectively manipulate light waves and allow the construction of sensors based on refractive index changes. By combining 3D ordered macroporous materials with linear and nonlinear optical materials, it is even possible to tune optical interactions, which could be technologically relevant for organic light-emitting diodes (OLEDs), organic photovoltaics (OPVs), lasers, electro-optical modulators, and optical switches.

Much research remains to be performed on the unique structural and optical properties of 3D ordered macroporous materials. Accessible and economic fabrication of these materials is essential to achieve this. 3D lithographic techniques provide high quality structures but are expensive and inaccessible to most researchers.[7,8] A more economical method to fabricate 3D ordered macroporous materials is by self-assembling colloids, resulting in so-called opals.[9] A templating strategy is often used to introduce additional functionality inside the porous structure, resulting in inverse opals.[2,3,10,11] Various fabrication methods for organic and inorganic inverse opals that display fluorescence,[12−19] nonlinear optics,[20−22] magneto-optics,[23−26] plasmonics,[27,28] or upconversion,[29−33] can be found in literature. Mostly, the template is first infiltrated with a solution, a sol−gel, or a melt and then removed by chemical etching or decomposition at high temperature. If no precautions are taken, this approach will automatically lead to the deposition of superfluous material on top of the template (overlayer).[34−38] The unwanted optical effects of the overlayer, which can be removed at the cost of an additional polishing or controlled etching step, limit their use in linear and nonlinear optics[34,35] and in membrane science and catalysis.[39] Some methods succeed in reducing the thickness of the overlayer by using a specially designed flow cell[40,41] or by containing the templating material between slides.[42−45] For the fabrication of inorganic inverse opals, alternative infiltration methods such as chemical vapor deposition (CVD), atomic layer deposition (ALD), or electrodeposition are available, yet they also require careful parameter control to avoid overlayers. A different approach toward inverse opals is coself-assembly of the template and the templating material. Hatton et al. successfully employed this method to fabricate overlayer-free inorganic inverse opals.[39] Like CVD and ALD, their method involved high temperature steps, preventing its use in making organic inverse opals. In analogy with electrodeposition, electropolymerisation is viable to fabricate organic inverse opals without overlayer by correct timing.[46−50] However, being

Received: October 31, 2013
Accepted: February 21, 2014
Published: February 21, 2014

   dx.doi.org/10.1021/am4048464 | ACS Appl. Mater. Interfaces 2014, 6, 3870−3878

based on electrochemical methods, it is suitable only for a limited number of substrates and templating materials.

In this work, we developed a straightforward and versatile method to fabricate highly uniform polymer inverse opals without overlayer. Briefly, our approach consists of sandwiching a resin melt between two opal templates, forcing all material inside or between the macroporous structures. The opal voids are fully filled, and the superfluous melt material is extruded before curing the resin. Finally, the opal templates are removed by chemical etching. The resulting structures are freestanding 3D macroporous films with large-area uniformity, displaying strong photonic properties due to their structural order.

Additionally, many applications require specific optical functionalities. The versatility of our templating method is uniquely suited for this purpose as it allows doping of the melt before infiltration. Therefore, we can incorporate a large variety of optical functions in the inverse opals using a single approach. We demonstrated the versatility and power of our fabrication method by synthesizing inverse opals featuring fluorescence, chirality, upconversion, second harmonic generation, and third harmonic generation. The clear suppression of fluorescence by the photonic band gap further proves that the dopants are well integrated in the structure.

The novel aspects of our method are the automatic absence of overlayers and the broad choice of introducible (optical) functions. We are therefore confident that this work will facilitate research on inverse opals in general and on linear and nonlinear optical effects in 3D photonic crystals specifically. The relative ease of synthesis makes it accessible to most researchers. As a wide variety of materials can be fabricated, it will help the systematic investigation and improvement of existing effects in these structures, while providing a platform for the discovery and demonstration of novel effects.

2. MATERIALS AND METHODS

2.1. Polymer Inverse Opals. Silica nanoparticles of various sizes were obtained by performing temperature-controlled Stöber-Fink-Bohn syntheses.[51] After purification, convective self-assembly was used to assemble these silica nanoparticles into artificial opals (4 g/L in ethanol at 37 °C; further details can be found in Supporting Information).[52] The inversion of the silica opals was performed using a templating approach. The epoxy monomer (Bisphenol A diglycidyl ether (DGEBA), Momentive, United States) was degassed in vacuum and mixed with the resin hardener (4,4′-Methylenedianiline, ≥97.0%, Sigma Aldrich) in a 2:1 molar ratio at 100 °C, resulting in an equal amount of functionalities. At this moment, the curing starts and the viscosity of the mixture slowly starts to increase. As low viscosity is preferred to achieve complete filling and to extrude as much superfluous material as possible, the infiltration should be done directly after mixing. A drop of resin melt was sandwiched between two silica opals on thin glass slides, and the superfluous material was extruded by pressing both glass slides together. The outsides of the sandwich structure were cleaned with chloroform (99.8%, Acros Organics, Belgium), and the structure was left to cure (typically around 70−100 °C, >4 h). After curing, the thin glass slides and the silica nanoparticles were etched away with a solution of hydrogen fluoride (±24 h, 10% HF, Sigma-Aldrich, United States) in water. After etching, the freestanding inverse opal films were rinsed with Milli-Q and methanol (analytic grade, Fisher Chemical, United States) and dried at ambient conditions.

2.2. Doping of the Polymer Inverse Opals. To introduce specific functionality in the inverse opals, the epoxy monomer should be uniformly mixed with the appropriate dopant before following the procedure described above. To ensure uniform mixing, the monomer and the dopant were dissolved/dispersed in a common solvent (chloroform). The solvent was then removed by rotary evaporation (Buchi rotavapor R-210 with heating bath B-491 and Vacuubrand CVC 3000 vacuum pump). Details on the doping of the specific molecules or nanoparticles and on the equipment used for optical and structural characterization can be found in the Supporting Information.

3. RESULTS AND DISCUSSION

3.1. Fabrication of Inverse Opals. We developed a straightforward method to fabricate uniform, freestanding polymer inverse opals (Figure 1). The absence of solvents

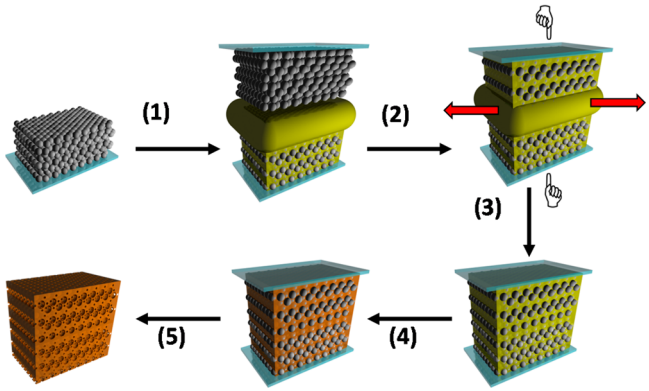

Figure 1. The fabrication method of inverse opals involves 5 steps. (1) Infiltration with resin melt at 100 °C. (2) Introduction and infiltration of a second opal. (3) Extrusion of superfluous resin melt by applying pressure. (4) Curing at 100 °C for more than 4 h. (5) Etching of silica with 10% HF.

and the low viscosity during infiltration ensure that the resin melt fully fills the voids of the silica opal templates, leading to a good conservation of the structural properties after inversion. This can clearly be seen from an electron microscopy image taken of a sample where the top layers of the inverse opal were removed, allowing us to visualize the interior structure (Figure 2a). The small pores that connect the spherical air voids can be

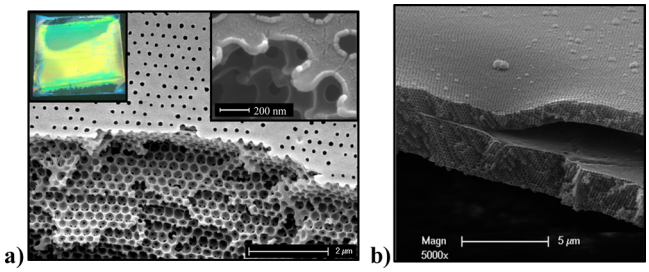

Figure 2. (a) The inverse opal is a good replication of the original fcc crystal. The presence of pores indicates etching throughout the whole structure (right inset). On the macroscopic scale, it is a freestanding film with large-area uniformity (left inset). (b) A cross-section shows the absence of overlayers on both sides of the film.

clearly seen. The cracks visible on the surface at high magnification originate from the gold layer that was sputtered on the sample for imaging purposes. The inverse opals are macroscopically uniform for at least a few square centimeters (Figure 2a, left inset).

The featured fabrication method does not require sintering or polishing. A sintering step is often necessary to partially melt the original silica or polystyrene spheres together (necking).[18,34,36−38,53−57] Without necking, many fabrication methods suffer from inefficient etching as the etching solution (10%

dx.doi.org/10.1021/am4048464 | ACS Appl. Mater. Interfaces 2014, 6, 3870−3878

hydrogen fluoride, HF) needs to pass through the pores to remove the template material. In our method, the etching solution can pass through the resin itself without compromising the structural integrity, making sintering steps redundant. Moreover, an overlayer is often formed by superfluous templating material on top of the inverse opal. This increases the background signal of many linear and nonlinear optical effects and even influences the spectral position of the photonic band gap.[58] Our sandwich approach prevents the presence of such polymer overlayers (Figure 2b), eliminating the need for additional polishing steps as well. This is a logical result of the fact that the silica opals are directly attached to the material they were assembled on, which are necessarily on the outside of the sandwich structure. The absence of a polymer overlayer is especially important in the study of optical effects in inverse opals. It ensures all the optically active material is either inside or between the photonic crystal structure and hence maximizes photonic band gap or band edge effects. It should be noted that there is a polymer interlayer at some positions of the sample (see Supporting Information). We attribute the appearance of this interlayer to the limited flatness of the colloidal crystals after convective self-assembly, which locally prevents the complete extrusion of superfluous melt material. These local interlayers should be eliminated when employing assembly methods with better thickness uniformity, e.g., spincoating and Langmuir–Blodgett techniques.[8]

If required, the curing temperature can be varied. The effects of temperature variation on the curing process was quantified using differential scanning calorimetry (DSC) (Figure 3). With

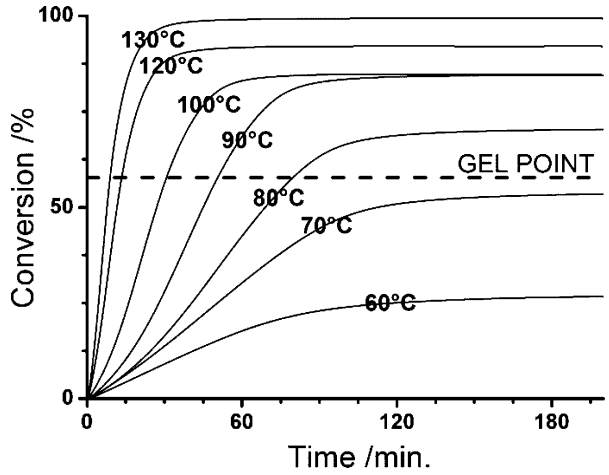

Figure 3. Lower curing temperatures increase the required curing time but decrease the maximum achievable conversion of DGEBA monomer into a networked epoxy. The theoretical gel point is indicated by the horizontal dashed line.

decreasing temperature, longer curing times are needed to reach maximum conversion of the monomer into a networked epoxy. The maximum achievable conversion is lower at lower temperatures as well. This can be explained by gradual increase in glass transition temperature (T_g) during the curing process. When the T_g reaches the curing temperature, the mobility of the system is drastically decreased. At this point, the reaction stops, resulting in a partially cured epoxy resin. Lower curing temperatures thus result in lower final conversion. The gel point, determined as the minimum conversion where a polymer chain reaches a theoretical infinite molecular weight, was estimated by using the Flory–Stockmayer equation[59] to be 57.7%. The DSC measurements therefore suggest that cross-linking is ensured when curing at temperatures above 80 °C. Below the gel point, the viscosity will gradually decrease. More details on the calculation of conversion efficiencies can be found in Supporting Information.

3.2. Optical Characterization and Reproducibility. During the whole inversion process, the filling and etching can be followed visually and spectroscopically.[60,61] A typical example of the changes in the extinction spectrum at normal incidence after the different process steps is shown in Figure 4a. The infiltration with resin melt (n = 1.676) leads to an increase in the effective refractive index (n_{eff}) and hence a red shift of the photonic band gap maximum (λ_{max}), as can be seen from the Bragg formula for fcc close-packed systems near normal incidence:[8]

$$\lambda_{max} = 2d_{[111]}\sqrt{{n_{eff}}^2 - \sin^2\theta_{[111]}} \quad (1)$$

with $\theta_{[111]}$, the angle between the incident light beam (in air) and the [111] direction, and $d_{[111]}$, the spacing between the (111) planes, which is from geometrical considerations (see Supporting Information), equal to $(2/3)^{1/2}$ times the sphere diameter.

The refractive index contrast is reduced as well, weakening the photonic band gap. The opposite is observed during the etching step; the silica phase (n = 1.45) is replaced by air (n = 1), thus strongly reducing the effective refractive index and blue shifting the photonic band. The increased refractive index contrast strengthens the photonic band gap effect.

The spectral position of the photonic band gap was used to estimate the reproducibility of our sandwiching approach (Figure 4b). We self-assembled 18 opals from 307.17 ± 10.62 nm (as determined with transmission electron microscopy, see Supporting Information) silica nanoparticles and used them to make 9 sandwich structures. Extinction spectra were taken directly after self-assembly, after curing, and after etching, and the positions of the peak maxima were determined by peak fitting with Lorentz functions. The average peak positions were respectively, 678.5 ± 8.4, 750.2 ± 16.0, and 610.5 ± 6.7 nm. The increase in standard deviation after filling was attributed to a larger inaccuracy when fitting these weaker peaks. These experimental results were then compared with the peak maxima predicted by Bragg's Law at normal incidence. For these calculations, the effective refractive index was estimated by

$${n_{eff}}^2 = \sum_i f_i {n_i}^2 \quad (2)$$

and constant filling fractions (f_i) of 0.74 and 0.26 (due to the close-packed fcc crystal structure) were assumed in all fabrication steps. As shown in Figure 4b, the experimental peak maxima (black) match well with the calculated ones (red). The uncertainty on the calculations is a direct result of the standard deviation on the particle size.

Like classic opals, our sandwich structures display strong iridescence. The band gap maxima obtained from angular extinction measurements are easily fitted by Bragg's law (Figure 5). When going to large angles, a second Bragg resonance appears and eventually masks the photonic band gap originating from the (111) planes (see Supporting Information). This second peak is well described in literature and originates from reflections on the (200) planes.[62−64] More

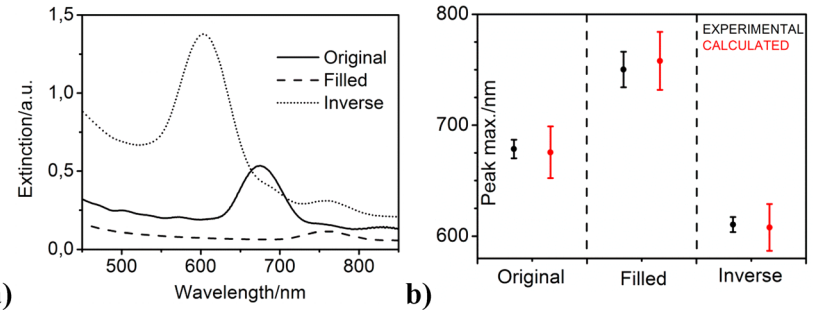

Figure 4. (a) As the effective refractive index is altered, the position of the photonic band gap shifts during the inversion procedure. The strength of the photonic band gap is modified as well because of the changes in refractive index contrast and filling fractions. (b) The experimentally determined peak maxima (black) agree well with those calculated using the Bragg formula (red).

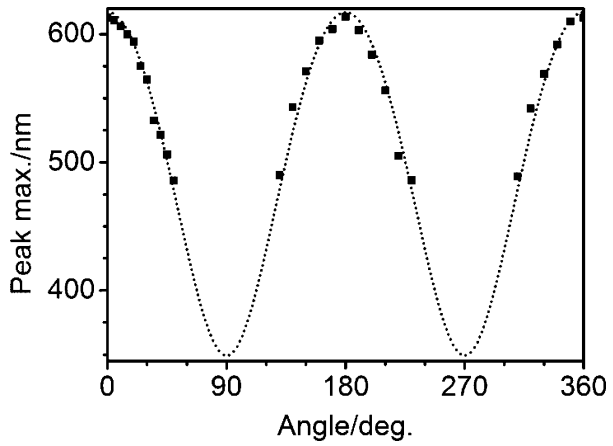

Figure 5. The photonic band gap is strongly angle dependent and fits well to the angular Bragg equation.

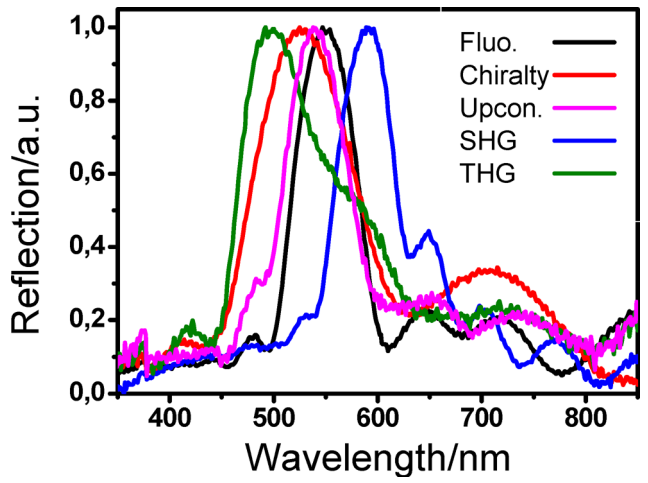

Figure 6. All studied inverse opals display strong selective reflection in addition to their specific optical function.

details on the calculation methods and parameters used in this section can be found in Supporting Information.

3.3. Doping of Inverse Opals. A myriad of optical functionalities can be introduced by doping the resin melt before infiltration. In this paper, we demonstrate fluorescence suppression, chirality, upconversion, third harmonic generation (THG), and second harmonic generation (SHG) in inverse opals (see Sections 3.4−3.7). In addition to the optical effects introduced by doping, there is still a strong selective reflection due to the structural properties of the inverse opal (Figure 6). The presence of both structural and introduced optical effects in a single structure opens many possibilities toward the study of band gap and slow light effects.[8,65]

Although the options for doping are plentiful, there are some constraints to consider. First, heat stability might be an issue for some dopants. This problem can be solved by lowering the curing temperature and prolonging the curing time (see Section 3.1). Second, the dopants should be sufficiently chemically compatible with the epoxy monomer to avoid aggregation effects and should be resistant to HF, as it can freely pass through the cured resin. The chemical compatibility could be tailored by changing the nature of the epoxy monomer or the nature of the dopant itself, e.g., by appropriate functionalization of nanoparticles (see Section 3.6).

3.4. Fluorescence Suppression. The inverse opals doped with fluorescent coumarin 343 clearly display angle-dependent fluorescence suppression. Fluorescence suppression is a well-known band gap effect that has been studied in opals[13,14,18,25,66−72] and inorganic[13,14,17,19] and organic inverse opals.[18] The reduced density of states in the photonic band gap decreases the efficiency of radiative decay. As the photonic band gap in the inverse opals is also angle dependent, the spectral form of the fluorescence is different for different detection angles. In this experiment, we compared the fluorescence spectrum of a sandwich structure with a band gap outside the fluorescence peak (indicated as the reference) with that of a sandwich structure whose band gap coincides with the fluorescence peak (indicated as the active sample). In both samples, the coumarin 343 is embedded in the epoxy and the emitted light travels through material of the same average refractive index (not considering anomalous dispersion near the band gap). The only difference is the size of the air voids and hence the position of the band gap. The reference sample did not display strong angle-dependent fluorescence as the spectral shape remained roughly the same (Figure 7a). The active sample did show a strong modification of the fluorescence spectrum when observed under different angles (Figure 7b). The angular dependence of the band gap itself was measured with UV−vis spectrophotometry. It should be noted that we used sandwich structures containing no dye but having the same band gap position at normal incidence to measure the angle dependence of the band gap. This was necessary because the absorption of coumarin 343 masked the photonic band gap at higher angles (data not shown). The inset of Figure 5b shows that the measured peak maxima follow the angle-dependent Bragg law (see Section 3.1). The vertical dashed lines in Figure 5b represent the calculated peak maxima for the

dx.doi.org/10.1021/am4048464 | ACS Appl. Mater. Interfaces 2014, 6, 3870−3878

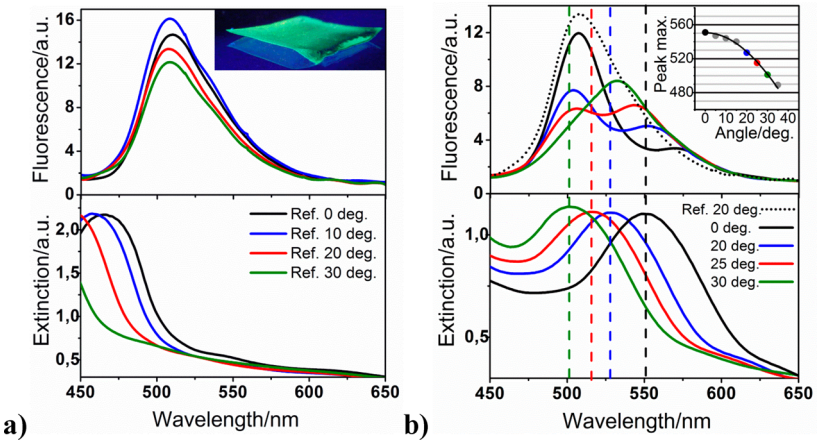

Figure 7. (a) The fluorescent coumarin 343 is uniformly doped in the inverse opal (inset). The reference sample had a band gap outside the spectral range of fluorescence. No significant shape changes were observed in its fluorescence spectrum when changing the detection angle. (b) In the active sample, the fluorescence spectrum (top) changes shape when detected under different angles. This is caused by selective suppression by the photonic band gap (bottom), which is angle dependent. The dotted lines show the calculated band gap positions at different angles. These calculations match well with the experimentally determined peak maxima (inset).

color coded angles and elucidate the good correspondence between the calculated peak maxima, the measured band gaps, and the positions of fluorescence suppression. At an angle of 25 degrees, the band gap of the active sample coincided with the wavelength of maximal fluorescence, resulting in a clear dip in the fluorescence spectrum. As fluorescence suppression is a direct result of the anomalous dispersion of the photonic crystal, these results clearly indicate that the dopants are indeed embedded in the photonic structure itself.

3.5. Chirality. To emphasize the versatility of our fabrication method, we also doped chiral clusters in inverse opals. The chiral entities were enantiomerically pure 2,2′-bis(diphenylphosphino)-1,1′-binaphthyl (BINAP) molecules attached to gold nanoparticles.[73] As the crystal structure of the inverse opals themselves is anisotropic, care has to be taken to separate the effects of anisotropy and chirality. By averaging the results of circular dichroism measurements over multiple azimuthal angles and both directions of propagation, the contributions of anisotropy were canceled out.[74] The (R) and (S) forms of the chiral molecules show opposite average circular dichroism (CD) (Figure 8), confirming that the resulting inverse opals are chiral. The combination of photonic crystals and chirality is especially interesting for creating negative refractive index materials[75−77] and, when combined with fluorescence, for lasing applications.[78] Usually, the chirality is introduced by a chiral supramolecular structure that displays different band gaps for left and right handed circular polarized light.[79−82] In our case, not the crystal structure itself but the dopants are chiral. The effect of the band gap on the chiral signal remains to be investigated.

3.6. Upconversion. The doping procedure is also suitable to introduce nonlinear optical functionality. First, we demonstrate upconversion in our inverse opals, i.e., the conversion of longer to shorter wavelengths through excited state absorption (ESA) processes.[83] $NaGdF_4:Yb^{3+},Er^{3+}$ nanoparticles with an average size of 17.5 ± 1.0 nm were used for this purpose. These particles are small enough to pass through the pores of the original template. To avoid aggregation in the epoxy monomer, the surface of the nanoparticles was silanized with (2-phenylethyl)trimethoxy-silane.[84] When exposed to 980 nm laser light, the Yb(III)-ions in the nanoparticles get excited

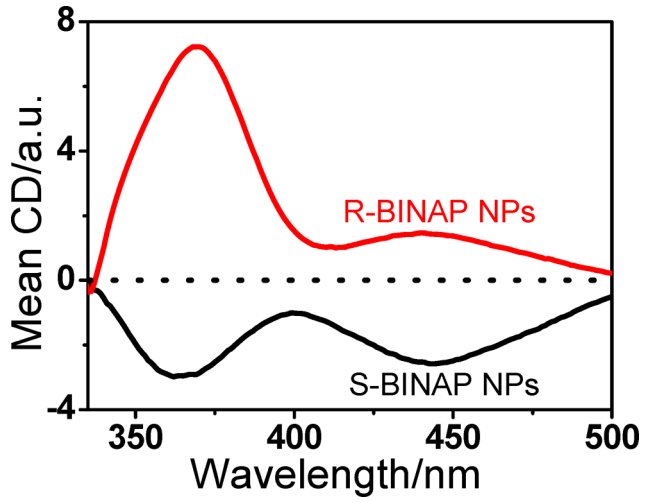

Figure 8. The circular dichroism is nonzero after averaging over all azimuthal angles. Together with the opposite response of both enantiomers, this proves the presence of chirality in the inverse opals.

to a higher energy level and efficiently transfer the energy to nearby Er(III)-ions. When the higher energy levels of the Er(III)-ions get populated via the ESA system, they relax by emitting shorter wavelength photons. The characteristic luminescent peaks corresponding to blue (408 nm) and green (526 and 553 nm) color were observed when exposing our doped inverse opals to a 980 nm laser, proving the effective integration of the nanoparticles in the inverse opal structure (Figure 9).

3.7. Frequency Tripling and Doubling. Third harmonic generation (THG), or frequency tripling, was achieved by doping with Buckminster-fullerene. Because the electrons are strongly delocalized, fullerene has a high polarizability and hence a high molecular third order susceptibility.[85−88] Indeed, a strong peak was observed at 400 nm when the fullerene inverse opal was probed with 1200 nm laser light (Figure 10a). Second harmonic generation (SHG), or frequency doubling, is slightly more complex as symmetry considerations have to be taken into account. SHG can only occur in the absence of centrosymmetry, both at the molecular and the bulk level.[89]

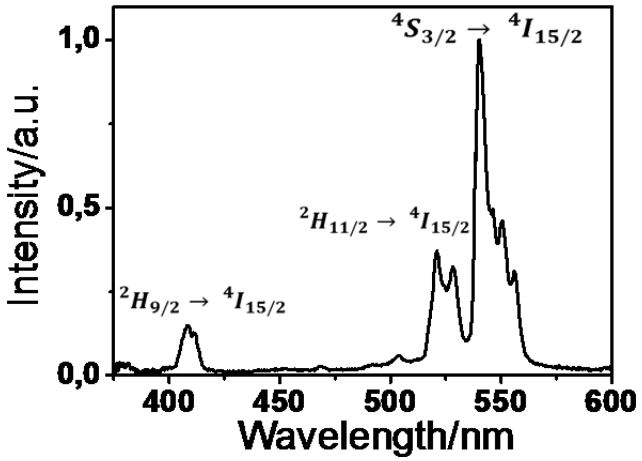

Figure 9. The luminescence spectrum from an inverse opal containing $NaGdF_4$:Yb^{3+},Er^{3+} nanoparticles clearly displays the characteristic blue and green upconversion peaks upon excitation with 980 nm light.

We used para-nitroanaline (PNA), a classic dipolar SHG dye, as the dopant.[90] After the inversion procedure, the PNA molecules are isotropically distributed in the cured epoxy resin. A modified version of corona poling was employed to orient the molecules and hence break the macroscopic centrosymmetry. The mobility of the PNA molecules was not achieved by heating the sample to the glass temperature of the polymer, as is commonly done, but by temporary solvation with chloroform. No dye leaked out of the structure during this process, which indicates that the molecules are trapped within the resin but still mobile enough to reorient. In a sense, we combined a well-known poling technique from the field of organic nonlinear optics with the structural properties of photonic crystals. This led to an inverse opal showing second harmonic generation (Figure 10b). These nonlinear optical inverse opals will be investigated further as the anomalous dispersion in such structures is believed to cause phase matching effects, which considerably boost the efficiency of nonlinear scattering effects.[21,91−96]

4. CONCLUSIONS AND PERSPECTIVES

We have developed a new and versatile fabrication method to fabricate freestanding polymer inverse opals. The resulting structures have large-area uniformity and lack overlayers. To prove the versatility of this method, fluorescence, chirality, upconversion, and frequency tripling and doubling were demonstrated in inverse opals. The presence of strong fluorescence suppression confirms that the dopants are well integrated in the photonic structure. The described fabrication method is especially well suited for investigating the effect of the band gap and band edge on linear and nonlinear optical effects as it combines both structural and inherent optical functions.

To include dopants that are not resistant to HF (e.g., magnetic iron oxide particles), toluene or other organic solvents could be used in combination with templates self-assembled from polystyrene particles. Although such strategies have been successfully employed in literature,[40,97,98] additional research is needed to check compatibility with our fabrication method. When extrusion of the templating material was incomplete, an interlayer was present in our sandwich structures. This effect could be harnessed to make defect modes in a single fabrication step. By varying the viscosity of the melt (temperature) or the amount of applied pressure during melt extrusion, we aim to accurately control the exact thickness of this interlayer. In combination with the possibility to dope, such thickness controlled microcavities would be technologically relevant to steer the optical processes in OLEDS, OPVs, lasers, electro-optical modulators, and optical switches.

■ ASSOCIATED CONTENT

Supporting Information

Details on the synthesis of silica nanoparticles and convective self-assembly. Details on the doping of epoxy monomer and synthesis of dopants (if applicable). Details on the structural and optical characterization. SEM picture of inverse opal with local interlayer. Details on the parameters used in the Bragg equation. Details on the calculation of epoxy conversion percentages. This material is available free of charge via the Internet at http://pubs.acs.org/.

■ AUTHOR INFORMATION

Corresponding Authors

*E-mail: pieterjan.demeyer@fys.kuleuven.be.
*E-mail: koen.clays@fys.kuleuven.be. Tel: +3216327508.

Notes

The authors declare no competing financial interest.

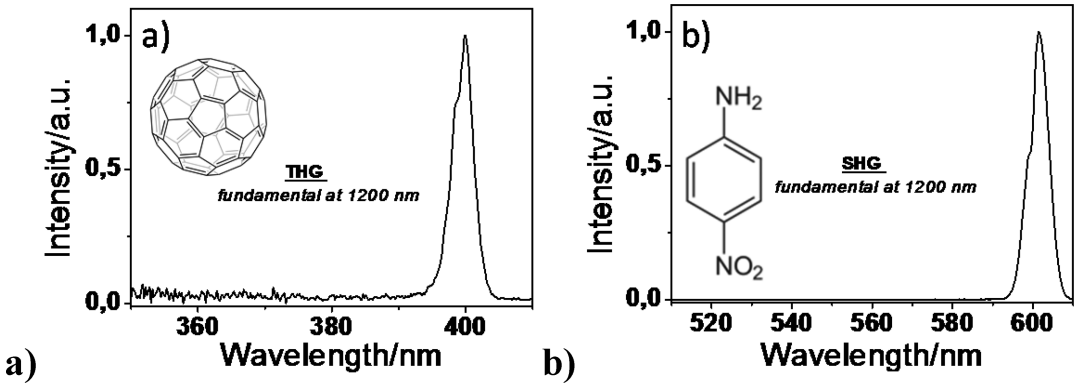

Figure 10. (a) A strong THG peak was observed at 400 nm when exposing the fullerene inverse opal to 1200 nm laser light. (b) When probed with 1200 nm laser light, the poled PNA inverse opal displayed a strong SHG peak around 600 nm.

■ ACKNOWLEDGMENTS

We are grateful to the University of Leuven (GOA and Research fund) for financial support. P.-J.D. thanks the KULeuven for his FLOF scholarship and his colleagues Ward Brullot, Maarten Bloemen, Koen Nuyts, Kuo Zhong, and Maarten Vanbel for the useful discussions. We would also like to thank Maarten Bloemen for the TEM measurements and Bram Vanroy for the dielectric spectroscopy experiment. S.V.C. (project number G092713N) and S.V. are grateful for financial support from the FWO-Vlaanderen. S.C. thanks IWT-Vlaanderen for her scholarship.

■ REFERENCES

(1) Stein, A.; Schroden, R. C. Colloidal Crystal Templating of Three-Dimensionally Ordered Macroporous Solids: Materials for Photonics and beyond. *Curr. Opin. Solid State Mater. Sci.* **2001**, *5*, 553−564.

(2) Wu, D.; Xu, F.; Sun, B.; Fu, R.; He, H.; Matyjaszewski, K. Design and Preparation of Porous Polymers. *Chem. Rev.* **2012**, *112*, 3959−4015.

(3) Thomas, A.; Goettmann, F.; Antonietti, M. Hard Templates for Soft Materials: Creating Nanostructured Organic Materials. *Chem. Mater.* **2008**, *20*, 738−755.

(4) Yu, J.-S.; Kang, S.; Yoon, S. B.; Chai, G. Fabrication of Ordered Uniform Porous Carbon Networks and Their Application to a Catalyst Supporter. *J. Am. Chem. Soc.* **2002**, *124*, 9382−9383.

(5) Collins, G.; Blömker, M.; Osiak, M.; Holmes, J. D.; Bredol, M.; O'Dwyer, C. Three-Dimensionally Ordered Hierarchically Porous Tin Dioxide Inverse Opals and Immobilization of Palladium Nanoparticles for Catalytic Applications. *Chem. Mater.* **2013**, *25*, 4312−4320.

(6) Wang, Y.; Caruso, F. Macroporous Zeolitic Membrane Bioreactors. *Adv. Funct. Mater.* **2004**, *14*, 1012−1018.

(7) Xia, Y.; Gates, B.; Yin, Y.; Lu, Y. Monodispersed Colloidal Spheres: Old Materials with New Applications. *Adv. Mater.* **2000**, *12*, 693−713.

(8) González-Urbina, L.; Baert, K.; Kolaric, B.; Pérez-Moreno, J.; Clays, K. Linear and Nonlinear Optical Properties of Colloidal Photonic Crystals. *Chem. Rev.* **2012**, *112*, 2268−2285.

(9) Kruglova, O.; Demeyer, P.-J.; Zhong, K.; Zhou, Y.; Clays, K. Wonders of Colloidal Self-Assembly. *Soft Matter* **2013**, *9*, 9072−9087.

(10) Wang, Y.; Price, A. D.; Caruso, F. Nanoporous Colloids: Building Blocks for a New Generation of Structured Materials. *J. Mater. Chem.* **2009**, *19*, 6451−6464.

(11) Stein, A.; Li, F.; Denny, N. R. Morphological Control in Colloidal Crystal Templating of Inverse Opals, Hierarchical Structures, and Shaped Particles. *Chem. Mater.* **2007**, *20*, 649−666.

(12) Fu, M.; Zhou, J.; Li, B.; Xiao, Q. F.; Wang, Y. H.; Li, L. T. Optical Properties of Nanocrystalline Ag Doped Silica Inverse Opals. *Key Eng. Mater.* **2007**, *336*−*338*, 555−557.

(13) Bechger, L.; Lodahl, P.; Vos, W. L. Directional Fluorescence Spectra of Laser Dye in Opal and Inverse Opal Photonic Crystals. *J. Phys. Chem. B* **2005**, *109*, 9980−9988.

(14) Koenderink, F.; Bechger, L.; Lagendijk, A.; Vos, W. L. An Experimental Study of Strongly Modified Emission in Inverse Opal Photonic Crystals. *Phys. Status Solidi A* **2003**, *197*, 648−661.

(15) Deng, L.; Wang, Y.; He, D. Modified Spontaneous Emission of Organic Molecules in-Filled in Inverse Opals. *J. Nanosci. Nanotechnol.* **2011**, *11*, 9749−9751.

(16) Brzezinski, A.; Lee, J.-T.; Slinker, J. D.; Malliaras, G. G.; Braun, P. V; Wiltzius, P. Enhanced Emission from fcc Fluorescent Photonic Crystals. *Phys. Rev. B* **2008**, *77*, 233106.

(17) Schriemer, H.; van Driel, H.; Koenderink, F.; Vos, W. Modified Spontaneous Emission Spectra of Laser Dye in Inverse Opal Photonic Crystals. *Phys. Rev. A* **2000**, *63*, 011801.

(18) Yoshino, K.; Lee, S. B.; Tatsuhara, S.; Kawagishi, Y.; Ozaki, M.; Zakhidov, A. A. Observation of Inhibited Spontaneous Emission and Stimulated Emission of Rhodamine 6G in Polymer Replica of Synthetic Opal. *Appl. Phys. Lett.* **1998**, *73*, 3506−3508.

(19) Lodahl, P.; Van Driel, F.; Nikolaev, I. S.; Irman, A.; Overgaag, K.; Vanmaekelbergh, D.; Vos, W. L. Controlling the Dynamics of Spontaneous Emission from Quantum Dots by Photonic Crystals. *Nature* **2004**, *430*, 654−657.

(20) Becker, C.; Linden, S.; von Freymann, G.; Tétreault, N.; Vekris, E.; Kitaev, V.; Ozin, G. A.; Wegener, M. Two-Color Pump−probe Experiments on Silicon Inverse Opals. *Phys. Status Solidi B* **2006**, *243*, 2354−2357.

(21) Fedyanin, A. A.; Aktsipetrov, O. A.; Kurdyukov, D. A.; Golubev, V. G.; Inoue, M. Nonlinear Diffraction and Second-Harmonic Generation Enhancement in Silicon-Opal Photonic Crystals. *Appl. Phys. Lett.* **2005**, *87*, 151111.

(22) Carvajal, J. J.; Peña, A.; Kumar, R.; Pujol, M. C.; Mateos, X.; Aguiló, M.; Díaz, F.; Vázquez de Aldana, J. R.; Méndez, C.; Moreno, P.; Roso, L.; Trifonov, T.; Rodríguez, A.; Alcubilla, R.; Král, Z.; Ferré-Borrull, J.; Pallarès, J.; Marsal, L. F.; Di Finizio, S.; Macovez, R.; Martorell, J. New Approaches for the Fabrication of Photonic Structures of Nonlinear Optical Materials. *J. Lumin.* **2009**, *129*, 1441−1447.

(23) Caicedo, J. M.; Pascu, O.; López-García, M.; Canalejas, V.; Blanco, Á.; López, C.; Fontcuberta, J.; Roig, A.; Herranz, G. Magnetophotonic Response of Three-Dimensional Opals. *ACS Nano* **2011**, *5*, 2957−2963.

(24) Caicedo, J. M.; Taboada, E.; Hrabovský, D.; López-García, M.; Herranz, G.; Roig, A.; Blanco, A.; López, C.; Fontcuberta, J. Facile Route to Magnetophotonic Crystals by Infiltration of 3D Inverse Opals with Magnetic Nanoparticles. *J. Magn. Magn. Mater.* **2010**, *322*, 1494−1496.

(25) Abramova, V. V; Slesarev, A.; Sinitskii, A. Synthesis of High-Quality Inverse Opals Based on Magnetic Complex Oxides: Yttrium Iron Garnet ($Y_3Fe_5O_{12}$) and Bismuth Ferrite ($BiFeO_3$). *J. Mater. Chem. C* **2013**, *1*, 2975−2982.

(26) Napolskii, K.; Sapoletova, N.; Eliseev, A.; Tsirlina, G.; Rubacheva, A.; Gan'shina, E.; Kuznetsov, M.; Ivanov, M.; Valdner, V.; Mishina, E.; van Etteger, A.; Rasing, T. Magnetophotonic Properties of Inverse Magnetic Metal Opals. *J. Magn. Magn. Mater.* **2009**, *321*, 833−835.

(27) Kuo, C.-Y.; Lu, S.-Y.; Chen, S.; Bernards, M.; Jiang, S. Stop Band Shift Based Chemical Sensing with Three-Dimensional Opal and Inverse Opal Structures. *Sens. Actuators, B: Chem.* **2007**, *124*, 452−458.

(28) Tan, Y.; Qian, W.; Ding, S.; Wang, Y. Gold-Nanoparticle-Infiltrated Polystyrene Inverse Opals: A Three-Dimensional Platform for Generating Combined Optical Properties. *Chem. Mater.* **2006**, *18*, 3385−3389.

(29) Yang, Z.; Yan, D.; Zhu, K.; Song, Z.; Yu, X.; Zhou, D.; Yin, Z.; Qiu, J. Modification of the Upconversion Spontaneous Emission in Photonic Crystals. *Mater. Chem. Phys.* **2012**, *133*, 584−587.

(30) Li, Z.-X.; Li, L.-L.; Zhou, H.-P.; Yuan, Q.; Chen, C.; Sun, L.-D.; Yan, C.-H. Colour Modification Action of an Upconversion Photonic Crystal. *Chem. Commun.* **2009**, 6616−6618.

(31) Yang, Z.; Yan, D.; Song, Z.; Zhou, D.; Yu, X.; Yang, Y.; Wang, R.; Wu, H.; Yin, Z.; Qiu, J. Preparation and Upconversion Emission Properties of Y_2O_3: Er, Yb Inverse Opal. *Symp. Photonics Optoelectron.* **2012**, 1−3.

(32) Zhengwen, Y.; Zhu, K.; Song, Z.; Yu, X.; Zhou, D.; Yin, Z.; Yan, L.; Jianbei, Q. Photonic Band Gap and Upconversion Emission Properties of Yb, Er Co-Doped Lead Lanthanum Titanate Inverse Opal Photonic Crystals. *Appl. Phys. A: Mater. Sci. Process.* **2011**, *103*, 995−999.

(33) Zhang, F.; Deng, Y.; Shi, Y.; Zhang, R.; Zhao, D. Photo-luminescence Modification in Upconversion Rare-Earth Fluoride Nanocrystal Array Constructed Photonic Crystals. *J. Mater. Chem.* **2010**, *20*, 3895.

(34) Míguez, H.; Meseguer, F.; López, C.; López-Tejeira, F.; Sánchez-Dehesa, J. Synthesis and Photonic Bandgap Characterization of Polymer Inverse Opals. *Adv. Mater.* **2001**, *13*, 393−396.

(35) Yang, H.; Jiang, P. Self-Cleaning Diffractive Macroporous Films by Doctor Blade Coating. *Langmuir* **2010**, *26*, 12598−12604.

(36) Yan, W.; Li, H.; Shen, X. Preparation and Characterization of Three-Dimensionally Ordered Macroporous Styrene/p-Methylstyrene Syndiotactic Copolymer. *Eur. Polym. J.* **2005**, *41*, 992−995.
(37) Yan, W.; Li, H.; Shen, X. Three-Dimensionally Ordered Macroporous Syndiotactic Polystyrene: Preparation and Characterization. *Macromol. Rapid Commun.* **2005**, *26*, 564−568.
(38) Li, H.; Abraham, S.; Yan, W.; Ha, C.-S.; Kim, I. Synthesis and Conformation of Three-Dimensionally Ordered Macroporous Syndiotactic Polystyrene and Poly(p-Methyl Styrene). *Macromol. Rapid Commun.* **2007**, *28*, 1534−1539.
(39) Hatton, B.; Mishchenko, L.; Davis, S.; Sandhage, K. H.; Aizenberg, J. Assembly of Large-Area, Highly Ordered, Crack-Free Inverse Opal Films. *Proc. Natl. Acad. Sci.* **2010**, *107*, 10354−10359.
(40) Park, S. H.; Xia, Y. Macroporous Membranes with Highly Ordered and Three-Dimensionally Interconnected Spherical Pores. *Adv. Mater.* **1998**, *10*, 1045−1048.
(41) Gates, B.; Yin, Y.; Xia, Y. Fabrication and Characterization of Porous Membranes with Highly Ordered Three-Dimensional Periodic Structures. *Chem. Mater.* **1999**, *11*, 2827−2836.
(42) Lee, Y.-J.; Braun, P. V. Tunable Inverse Opal Hydrogel pH Sensors. *Adv. Mater.* **2003**, *15*, 563−566.
(43) Lee, Y.-J.; Pruzinsky, S. A.; Braun, P. V. Glucose-Sensitive Inverse Opal Hydrogels: Analysis of Optical Diffraction Response. *Langmuir* **2004**, *20*, 3096−3106.
(44) Huang, J.; Tao, C.; An, Q.; Zhang, W.; Wu, Y.; Li, X.; Shen, D.; Li, G. 3D-Ordered Macroporous Poly(ionic Liquid) Films as Multifunctional Materials. *Chem. Commun.* **2010**, *46*, 967−969.
(45) Jiang, P.; Hwang, K. S.; Mittleman, D. M.; Bertone, J. F.; Colvin, V. L. Template-Directed Preparation of Macroporous Polymers with Oriented and Crystalline Arrays of Voids. *J. Am. Chem. Soc.* **1999**, *121*, 11630−11637.
(46) Cassagneau, T.; Caruso, F. Semiconducting Polymer Inverse Opals Prepared by Electropolymerization. *Adv. Mater.* **2002**, *14*, 34−38.
(47) Yu, A.; Meiser, F.; Cassagneau, T.; Caruso, F. Fabrication of Polymer−Nanoparticle Composite Inverse Opals by a One-Step Electrochemical Co-Deposition Process. *Nano Lett.* **2003**, *4*, 177−181.
(48) Luo, X.; Killard, A. J.; Smyth, M. R. Nanocomposite and Nanoporous Polyaniline Conducting Polymers Exhibit Enhanced Catalysis of Nitrite Reduction. *Chem.−Eur. J.* **2007**, *13*, 2138−2143.
(49) Tian, S.; Wang, J.; Jonas, U.; Knoll, W. Inverse Opals of Polyaniline and Its Copolymers Prepared by Electrochemical Techniques. *Chem. Mater.* **2005**, *17*, 5726−5730.
(50) Grigoryeva, N. A.; Mistonov, A. A.; Napolskii, K. S.; Sapoletova, N. A.; Eliseev, A. A.; Bouwman, W.; Byelov, D. V; Petukhov, A. V; Chernyshov, D. Y.; Eckerlebe, H.; Vasilieva, A. V; Grigoriev, S. V. Magnetic Topology of Co-Based Inverse Opal-like Structures. *Phys. Rev. B* **2011**, *84*, 64405.
(51) Stöber, W.; Fink, A.; Bohn, E. Controlled Growth of Monodisperse Silica Spheres in the Micron Size Range. *J. Colloid Interface Sci.* **1968**, *26*, 62−69.
(52) Jiang, P.; Bertone, J. F.; Hwang, K. S.; Colvin, V. L. Single-Crystal Colloidal Multilayers of Controlled Thickness. *Chem. Mater.* **1999**, *11*, 2132−2140.
(53) Yoon, S. B.; Kang, S.; Yu, J.-S. Synthesis of Nanostructured Polymer Materials with Different Morphologies: Nanoporous Ordered Networks and Hollow Capsules. *Curr. Appl. Phys.* **2006**, *6*, 1054−1058.
(54) Hwang, S.; Lee, S.; Yu, J.-S. Template-Directed Synthesis of Highly Ordered Nanoporous Graphitic Carbon Nitride through Polymerization of Cyanamide. *Appl. Surf. Sci.* **2007**, *253*, 5656−5659.
(55) Blanco, A.; Míguez, H.; Meseguer, F.; López, C.; López-Tejeira, F.; Sanchez-Dehesa, J. Photonic Band Gap Properties of CdS-in-Opal Systems. *Appl. Phys. Lett.* **2001**, *78*, 3181−3183.
(56) Blanco, A.; Chomski, E.; Grabtchak, S.; Ibisate, M.; John, S.; Leonard, S. W.; López, C.; Meseguer, F.; Míguez, H.; Mondia, J. P.; Ozin, G. A.; Toader, O.; van Driel, H. M. Large-Scale Synthesis of a Silicon Photonic Crystal with a Complete Three-Dimensional Bandgap near 1.5 Micrometres. *Nature* **2000**, *405*, 437−440.
(57) Meseguer, F.; Blanco, A.; Míguez, H.; García-Santamaría, F.; Ibisate, M.; López, C. Synthesis of Inverse Opals. *Colloids Surf., A* **2002**, *202*, 281−290.
(58) Mihi, A.; Míguez, H.; Rodríguez, I.; Rubio, S.; Meseguer, F. Surface Resonant Modes in Colloidal Photonic Crystals. *Phys. Rev. B* **2005**, *71*, 125131.
(59) Flory, P. J. *Principles of Polymer Chemistry*; Cornell University Press: Ithaca, 1953.
(60) Demeyer, P.-J.; Bloemen, M.; Verbiest, T.; Clays, K. Tuning the Properties of Colloidal Magneto-Photonic Crystals by Controlled Infiltration with Superparamagnetic Magnetite Nanoparticles. *Proc. SPIE 8425, Photonic Crystal Materials and Devices X* **2012**, 84251R DOI: 10.1117/12.922299.
(61) Demeyer, P.-J.; Bloemen, M.; Verbiest, T.; Clays, K. Engineering of Colloidal Magneto-Photonic Crystals by Infiltration with Superparamagnetic Magnetite Nanoparticles. *Proc. Symp. IEEE Photonics Soc. Benelux* **2011**, 13−16.
(62) Van Driel, H. M.; Vos, W. L. Multiple Bragg Wave Coupling in Photonic Band Gap Crystals. *Phys. Rev. B* **2000**, *62*, 9872−9875.
(63) Romanov, S. G.; Maka, T.; Sotomayor Torres, C. M.; Müller, M.; Zentel, R.; Cassagne, D.; Manzanares-Martinez, J.; Jouanin, C. Diffraction of Light from Thin-Film Polymethylmethacrylate Opaline Photonic Crystals. *Phys. Rev. E* **2001**, *63*, 56603.
(64) Galisteo-López, J. F.; Palacios-Lidón, E.; Castillo-Martínez, E.; López, C. Optical Study of the Pseudogap in Thickness and Orientation Controlled Artificial Opals. *Phys. Rev. B* **2003**, *68*, 115109.
(65) Galisteo-López, J. F.; Galli, M.; Balestreri, A.; Patrini, M.; Andreani, L. C.; López, C. Slow to Superluminal Light Waves in Thin 3D Photonic Crystals. *Opt. Express* **2007**, *15*, 15342−15350.
(66) Vallée, R.; Baert, K.; Kolaric, B.; Van der Auweraer, M.; Clays, K. Nonexponential Decay of Spontaneous Emission from an Ensemble of Molecules in Photonic Crystals. *Phys. Rev. B* **2007**, *76*, 045113.
(67) Yablonovitch, E. Inhibited Spontaneous Emission in Solid-State Physics and Electronics. *Phys. Rev. Lett.* **1987**, *58*, 2059−2062.
(68) Yamasaki, T.; Tsutsui, T. Spontaneous Emission from Fluorescent Molecules Embedded in Photonic Crystals Consisting of Polystyrene Microspheres. *Appl. Phys. Lett.* **1998**, *72*, 1957.
(69) Baert, K.; Song, K.; Vallée, R. A. L.; Van der Auweraer, M.; Clays, K. Spectral Narrowing of Emission in Self-Assembled Colloidal Photonic Superlattices. *J. Appl. Phys.* **2006**, *100*, 123112.
(70) Blanco, A.; López, C.; Mayoral, R.; Míguez, H.; Meseguer, F.; Mifsud, A.; Herrero, J. CdS Photoluminescence Inhibition by a Photonic Structure. *Appl. Phys. Lett.* **1998**, *73*, 1781−1783.
(71) Kolaric, B.; Baert, K.; Van der Auweraer, M.; Vallée, R. A. L.; Clays, K. Controlling the Fluorescence Resonant Energy Transfer by Photonic Crystal Band Gap Engineering. *Chem. Mater.* **2007**, *19*, 5547−5552.
(72) Baert, K.; Kolaric, B.; Libaers, W.; Vallée, R. A. L.; Di Vece, M.; Lievens, P.; Clays, K. Angular Dependence of Fluorescence Emission from Quantum Dots inside a Photonic Crystal. *Res. Lett. Nanotechnol.* **2008**, *2008*, 1−4.
(73) Tamura, M.; Fujihara, H. Chiral Bisphosphine BINAP-Stabilized Gold and Palladium Nanoparticles with Small Size and Their Palladium Nanoparticle-Catalyzed Asymmetric Reaction. *J. Am. Chem. Soc.* **2003**, *125*, 15742−15743.
(74) Kuroda, R.; Harada, T.; Shindo, Y. A Solid-State Dedicated Circular Dichroism Spectrophotometer: Development and Application. *Rev. Sci. Instrum.* **2001**, *72*, 3802−3810.
(75) Pendry, J. B. A Chiral Route to Negative Refraction. *Sci.* **2004**, *306*, 1353−1355.
(76) Zhou, J.; Dong, J.; Wang, B.; Koschny, T.; Kafesaki, M.; Soukoulis, C. M. Negative Refractive Index due to Chirality. *Phys. Rev. B* **2009**, *79*, 121104.
(77) Zhang, S.; Park, Y.-S.; Li, J.; Lu, X.; Zhang, W.; Zhang, X. Negative Refractive Index in Chiral Metamaterials. *Phys. Rev. Lett.* **2009**, *102*, 23901.
(78) Furumi, S. Recent Progress in Chiral Photonic Band-Gap Liquid Crystals for Laser Applications. *Chem. Rec.* **2010**, *10*, 394−408.

(79) Vignolini, S.; Yufa, N. A.; Cunha, P. S.; Guldin, S.; Rushkin, I.; Stefik, M.; Hur, K.; Wiesner, U.; Baumberg, J. J.; Steiner, U. A 3D Optical Metamaterial Made by Self-Assembly. *Adv. Mater.* **2012**, *24*, OP23−OP27.
(80) Kuzyk, A.; Schreiber, R.; Fan, Z.; Pardatscher, G.; Roller, E.-M.; Hogele, A.; Simmel, F. C.; Govorov, A. O.; Liedl, T. DNA-Based Self-Assembly of Chiral Plasmonic Nanostructures with Tailored Optical Response. *Nature* **2012**, *483*, 311−314.
(81) Mille, C.; Tyrode, E. C.; Corkery, R. W. Inorganic Chiral 3-D Photonic Crystals with Bicontinuous Gyroid Structure Replicated from Butterfly Wing Scales. *Chem. Commun.* **2011**, *47*, 9873−9875.
(82) Thiel, M.; Wegener, M.; von Freymann, G. Layer-by-Layer Three-Dimensional Chiral Photonic Crystals. In *Conference on Lasers and Electro-Optics/Quantum Electronics and Laser Science Conference and Photonic Applications Systems Technologies*; Optical Society of America: San Jose, CA, 2008; p CWO4.
(83) Auzel, F. Upconversion and Anti-Stokes Processes with f and d Ions in Solids. *Chem. Rev.* **2003**, *104*, 139−174.
(84) Bloemen, M.; Brullot, W.; Luong, T.; Geukens, N.; Gils, A.; Verbiest, T. Improved Functionalization of Oleic Acid-Coated Iron Oxide Nanoparticles for Biomedical Applications. *J. Nanopart. Res.* **2012**, *14*, 1−10.
(85) Blau, W. J.; Byrne, H. J.; Cardin, D. J.; Dennis, T. J.; Hare, J. P.; Kroto, H. W.; Taylor, R.; Walton, D. R. M. Large Infrared Nonlinear Optical Response of C_{60}. *Phys. Rev. Lett.* **1991**, *67*, 1423−1425.
(86) Ganeev, R. A.; Ryasnyanskii, A. I.; Kulagin, I. A.; Usmanov, T. Generation of the Third Harmonic in Fullerene-Containing Polyimide Films by Picosecond Radiation of the Nd: YAG Laser. *Tech. Phys.* **2001**, *46*, 1270−1273.
(87) Gong, Q.; Sun, Y.; Xia, Z.; Zou, Y. H.; Gu, Z.; Zhou, X.; Qiang, D. Nonresonant Third-Order Optical Nonlinearity of All-Carbon Molecules C_{60}. *J. Appl. Phys.* **1992**, *71*, 3025−3026.
(88) Wang, Y.; Cheng, L. T. Nonlinear Optical Properties of Fullerenes and Charge-Transfer Complexes of Fullerenes. *J. Phys. Chem.* **1992**, *96*, 1530−1532.
(89) Verbiest, T.; Clays, K.; Rodriguez, V. *Second-Order Nonlinear Optical Characterization Techniques: An Introduction*; CRC Press: Boca Raton, 2009.
(90) Baraniraj, T.; Philominathan, P.; Vijayan, N. Growth and Characterization of Nonlinear Optical Para-Nitroaniline (pNA) Single Crystals. *Mod. Phys. Lett. B* **2007**, *21*, 2025−2032.
(91) Mingaleev, S.; Kivshar, Y. Nonlinear Photonic Crystals Toward All-Optical Technologies. *Opt. Photonics News* **2002**, *13*, 48.
(92) Martorell, J.; Vilaseca, R.; Corbalan, R. Second Harmonic Generation in a Photonic Crystal. *Appl. Phys. Lett.* **1997**, *70*, 702−704.
(93) Berger, V. Nonlinear Photonic Crystals. *Phys. Rev. Lett.* **1998**, *81*, 4136−4139.
(94) Saltiel, S.; Kivshar, Y. S. Phase Matching in Nonlinear $\chi^{(2)}$ Photonic Crystals. *Opt. Lett.* **2000**, *25*, 1204−1206.
(95) Soboleva, I. V.; Seregin, S. A.; Fedyanin, A. A.; Aktsipetrov, O. A. Efficient Bidirectional Optical Harmonics Generation in Three-Dimensional Photonic Crystals. *J. Opt. Soc. Am. B* **2011**, *28*, 1680.
(96) Maymo, M.; Martorell, J.; Molinos-Gomez, A.; Lopez-Calahorra, F. Visible Second-Harmonic Light Generated from a Self-Organized Centrosymmetric Lattice of Nanospheres. *Opt. Express* **2006**, *14*, 2864−2872.
(97) Wang, J. Y.; Cao, Y.; Feng, Y.; Yin, F.; Gao, J. P. Multiresponsive Inverse-Opal Hydrogels. *Adv. Mater.* **2007**, *19*, 3865−3871.
(98) Ueno, K.; Sakamoto, J.; Takeoka, Y.; Watanabe, M. Electrochromism Based on Structural Colour Changes in a Polyelectrolyte Gel. *J. Mater. Chem.* **2009**, *19*, 4778−4783.